High-Frequency Modeling of Permanent Magnet Synchronous Machines Using Grey Box Models

Hujun Peng, Niklas Driendl, Svetomir Stevic, *Graduate Student Member, IEEE*, Daniel Butterweck, Yousef Firouz, Leila Sharifian, and Kay Hameyer, *Senior Member, IEEE*

***Abstract*— A universal grey box model is proposed to model permanent magnet synchronous machines (PMSMs) with interior magnets for a wide frequency range. The proposed model supports the analysis of the parasitic effects in electrical drive between power electronics inverters, power cables, and electrical machines. Based on measured impedance spectra, equivalent electrical circuits are derived regarding the number of resonance points. A unique characteristic of the proposed grey box model lies in its flexibility, as it can be easily applied to model other electrical machines. Compared to the state-of-the-art, the proposed model considers a frequency-dependent mutual inductance between phases. The model parameters are fit using a differential evolution algorithm. Here, similarity between phases in high-frequency domain and the difference between phases in low-frequency domain are utilized for the parameterization process. The validation of the proposed grey box model is carried out in both the frequency and time domains. The proposed grey box model has a high degree of fidelity and can be used to estimate the maximum voltage stress in the insulation system of the analyzed PMSM.**

***Index Terms*— Converter machine interactions, electrical drive, electrical machine, high-frequency modeling, permanent magnet synchronous motor.**

I. Introduction

HAIRPIN windings are being increasingly utilized in automotive applications, as they enable significantly higher values of the copper fill factor compared to the state-of-the-art round conductors, thus improving the power density of electrical machines [1], [2]. The recent technological improvements of wide bandgap semiconductor materials, such as silicon carbide (SiC) and gallium nitride (GaN), have paved the way for the utilization of fast-switching metal–oxide–semiconductor field-effect transistor (MOSFET) in high-power applications. The MOSFET-based power semiconductor modules are used in automotive applications, thanks to their low switching losses, high switching frequency, and high-temperature endurance [3]. However, their relatively high-voltage slew rates lead to voltage oscillations in electrical machines [4], [5] as well as electromagnetic emissions [6]. These high-voltage oscillations occur due to the interaction between inverters, cables, and electrical machines [7].

The literature indicates that the maximum voltage in the electrical machines can reach up to two times the dc-link voltage due to the impedance mismatch between the power cables and the electrical machine in the case of applying a single pulse and up to quadruple the dc-link voltages in the case the double-pulsing effect occurs [8], [9], [10]. From this perspective, the common approach is to over-design the thickness of the insulation layers to avoid the failure of the insulation systems in electrical machines. In order to avoid the over-design of insulation systems, it is necessary to properly estimate the voltage peaks and their oscillation frequency at the terminals of electrical machines [11], [12], [13]. Additionally, the design of the insulation system must encompass the partial discharge phenomena [14]. To this end, high-frequency modeling of electrical machines can be employed to estimate the maximum voltage stress of electrical machines.

The high-frequency models refer to two types: the white box model and the grey box model. The white box model is based on the transmission-line model [15], which is implemented using an equivalent electrical circuit. The white box model of an electrical machine can be created before prototyping the machine, as merely geometry and material data are required to carry out the finite-element analysis (FEA). The equivalent electrical circuit is parameterized based on FEA results [16]. In [17], the frequency-dependent mutual impedance among neighboring conductors is implemented using current-controlled voltage sources. This method represents the state-of-the-art white box modeling of electrical machines. However, the implementation effort for the white box model is significant because FEA comes at a high computational load and it also requires the frequency-dependent permeability up to several megahertz [18].

The grey box modeling method can be used to analyze the interactions outside of the electrical machine. Compared to the white box model, the grey box modeling is used for already built electrical machines. The measured impedance spectra of the machine is utilized as an input for parametrization of the grey box model, which is implemented based on parameter search algorithms. To this end, the grey box modeling is useful during assembly of electrical drives to estimate the voltage stress on the insulation system of the electrical machine.

The state-of-the-art grey box models are well-developed for induction machines, surface-mounted permanent magnet synchronous machines (PMSMs), and electrical machines

Manuscript received 26 June 2023; revised 7 September 2023 and 9 November 2023; accepted 18 December 2023. Date of publication 7 February 2024; date of current version 27 December 2024. This work was supported by Toyota Motor Corporation. *(Corresponding author: Hujun Peng.)*

Hujun Peng, Niklas Driendl, Svetomir Stevic, Daniel Butterweck, and Kay Hameyer are with the Institute of Electrical Machines (IEM), RWTH Aachen University, 52062 Aachen, Germany (e-mail: hujun.peng@iem.rwth-aachen.de).

Yousef Firouz and Leila Sharifian are with Toyota Motor Europe, 1930 Zaventem, Belgium.

Digital Object Identifier 10.1109/TTE.2024.3363511

without rotors. In [19], a universal high-frequency model for induction motors is introduced. Fewer than four main resonance points are observed in the measured impedance spectra. In [20], high-frequency models are separately developed for differential-mode and common-mode voltages using stator core with windings. However, this model is validated only for a partially built electrical machine. In [21], the grey box model is presented for an induction motor, which represents the state-of-the-art for high-frequency modeling of induction machines. Compared to other publications, this model considers the mutual inductance between phases. However, the frequency dependence of the mutual inductance is not observed.

In [22] and [23], grey box models are developed for a surface-mounted PMSM and validated for the frequency range from 100 Hz to 10 MHz. The validation is based on test bench measurements regarding the common-mode voltage and current. However, the equivalent electrical circuit does not consider mutual impedance between phases. Moreover, the proposed grey box model lacks a physical basis, which affects the transferability of the model to other electrical machines. In [24] and [25], the mutual inductance between different coils of electrical machines is mentioned. However, the implementation of the frequency-dependent mutual inductance must be improved. In [26], the mutual inductance between different coils of an electric machine without a rotor and its frequency dependence is discussed. However, the simulated and measured inductance spectra are inconsistent.

In overall, the surface-mounted PMSM, induction machines, and electrical machines without rotor exhibit a strong magnetic symmetry between the d- and q-axes. The frequency-dependent mutual inductance between different phases is neglected during the grey box modeling of the induction machine and surface-mounted PMSM. This simplification does not strongly deteriorate the accuracy of the impedance modeling with respect to these electrical machines. However, as abovementioned, in the case of the PMSM with interior magnets, the self-inductance and the mutual inductance differ between different phases. Moreover, the grey box model for the PMSM with interior permanent magnets must consider the rotor position dependence because it influences the inductive coupling factors between different phases. It is also noteworthy to mention that the mutual impedance is frequency-dependent due to skin and proximity effects.

To close the gap in the grey box modeling of the PMSM, the following contributions are contained in this work.

1) Mutual inductance elements are introduced in the grey box model to consider the frequency-dependent mutual impedance between phases.
2) Each phase of the PMSM is individually modeled by considering the similarities between the phases at high frequencies and their differences at low frequencies.
3) Equivalent electrical circuits for representing the common mode and differential mode are integrated into a single electrical circuit.
4) The proposed grey box model is validated in the frequency domain up to 5 MHz.
5) The proposed grey box model is validated in the time domain based on test bench measurement results. The relative error is 3.75% regarding the peak value of the differential-mode voltage and the modeled oscillation frequency matches the measured frequency. The modeled common-mode voltage matches the measured voltage.

TABLE I
MOTOR TERMINAL CONFIGURATION FOR IMPEDANCE SPECTRUM MEASUREMENT

Symbol	Meaning
U-NP	Impedance between phase U and NP
V-NP	Impedance between phase V and NP
W-NP	Impedance between phase W and NP
U-GND	Impedance between phase U and GND
V-GND	Impedance between phase V and GND
W-GND	Impedance between phase W and GND
U-V	Impedance between phase U and phase V
V-W	Impedance between phase V and phase W
W-U	Impedance between phase W and phase U
U-VW	Impedance between phase U and phases VW
V-WU	Impedance between phase V and phases WU
W-UV	Impedance between phase W and phases UV

The organization of this article is as follows. In Section II, the measurement configuration and results are introduced. The difference in the impedance spectra in the low-frequency region and the similarity in the high-frequency region between phases are discussed. In Section III, the grey box modeling method is proposed. Section IV validates the model in the frequency domain by comparing the modeled and measured impedance spectra for different topologies. Then, Section V shows the validation results of the grey box model in the time domain based on test bench measurements. Finally, the conclusion is included in Section VI.

II. Measurement Setup and Results

The measurement of the electrical machine impedance at the stator terminals is required to parametrize the grey box model. To achieve a high degree of accuracy, the impedance measurement of various stator configurations and rotor positions is considered. In the following, the measurement setup as well as the impedance measurement results are presented.

A. Measurement Setup

The impedance analyzer "Keysight E4990A" is used to measure the impedance spectra in the frequency range from 100 Hz to 10 MHz. The measured amplitude and phase profiles as functions of frequency are recorded for various terminal connections of the PMSM under study, as provided in Table I and Fig. 1. The UV symbol denotes the short-circuit connection between terminals U and V, the symbol NP denotes the neutral point, and GND represents the housing. The PMSM studied in this article is mechanically adjusted so that its neutral point is accessible. The modeled PMSM is presented in Fig. 2. The rotor position of the studied PMSM is set by a stepper motor, thus enabling the impedance measurement at different rotor positions.

B. Impedance Measurement Results

The impedance spectra for the discussed configuration of the electrical machine terminals are illustrated in Fig. 3. The measurement results include the following impedance: phase-to-NP [Fig. 3(a)], phase-to-GND [Fig. 3(b)], and phase-to-phase [Fig. 3(c)]. It is noteworthy to mention that the

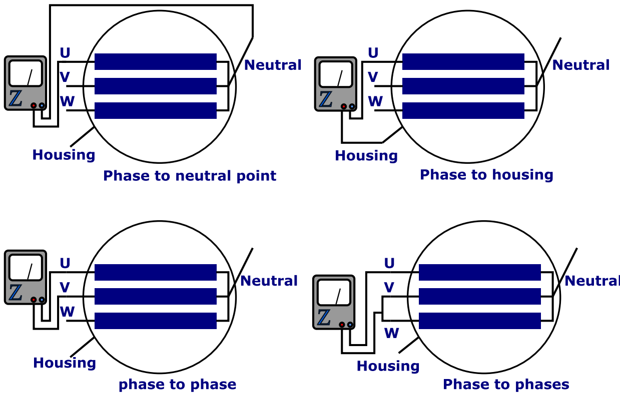

Fig. 1. Motor terminal configuration for impedance measurements.

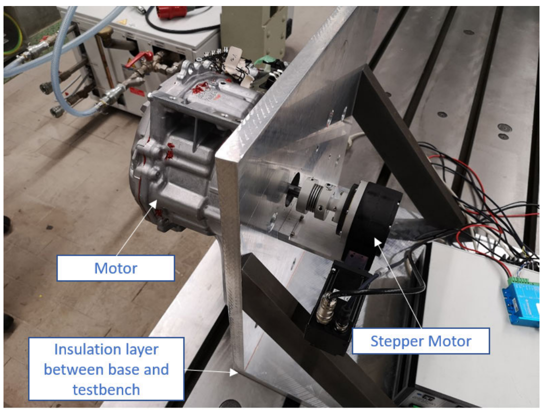

Fig. 2. Electrical motor to be measured.

measurement results shown in Fig. 3 are carried out in the configuration where the PMSM housing is placed on an insulated surface, here a wooden desk. The impact of placing the PMSM onto a grounded test bench will be discussed in detail in Section IV. In this section, the impedance spectra of the isolated PMSM are considered. At low frequencies, the impedance amplitude differs between the three phases due to the strong magnetic asymmetry between the d- and q-axes in the PMSM with internally buried magnets. On the other hand, the impedance spectra of different phases are almost identical at high frequencies since the impact of the magnetic asymmetry decreases with increasing frequency. Therefore, in creating the grey box model and its parameterization, the magnetic asymmetry in the low-frequency range and the magnetic symmetry in the high-frequency range must be regarded. Furthermore, there are six primary resonance points up to 5 MHz in the impedance spectra, as marked in Fig. 3(c). Section III will introduce a modular grey box model that captures all main resonance points in the impedance spectra.

III. Grey Box Model Setup and Choice of Optimization Parameters

A. Equivalent Electrical Circuit

Resonant points occur due to the interaction between the capacitances and inductances in a PMSM. Since there are six main resonant points, an electrical circuit with three branches is proposed, as illustrated in Fig. 4. The branches are numbered "0," "1," and "2." Branch 2 represents a part of a phase winding, which is close to the neutral point. Branch 0 represents the outermost part of a phase winding next to the machine terminal. Branch 1 describes the middle part, which

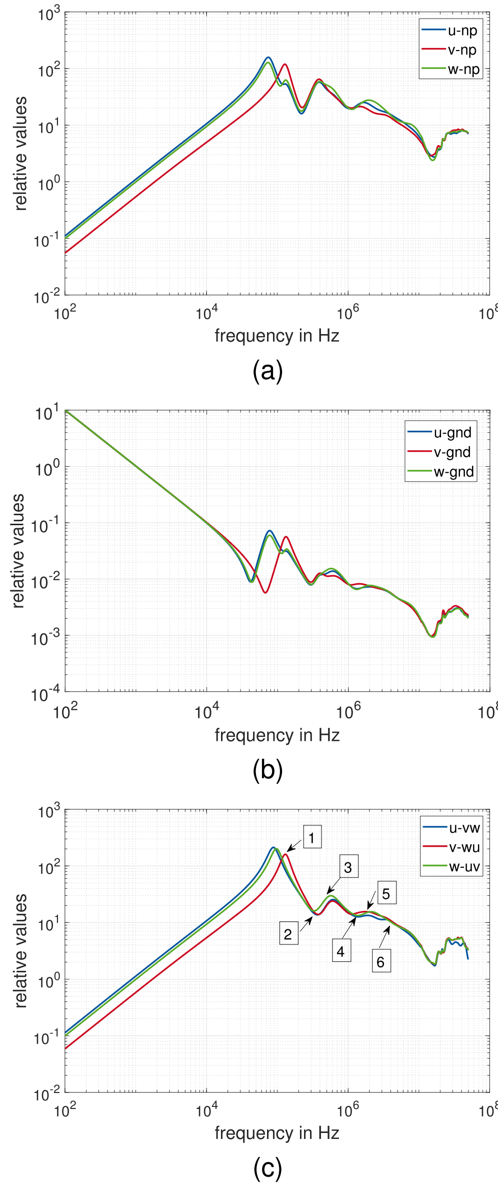

Fig. 3. Impedance spectra of different terminal configuration typologies: (a) phase-to-NP; (b) phase-to-housing; and (c) phase-to-phase.

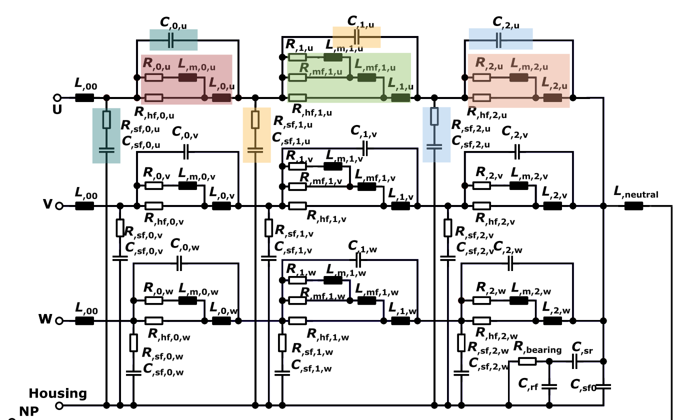

Fig. 4. Grey box model without mutual inductances between the phases.

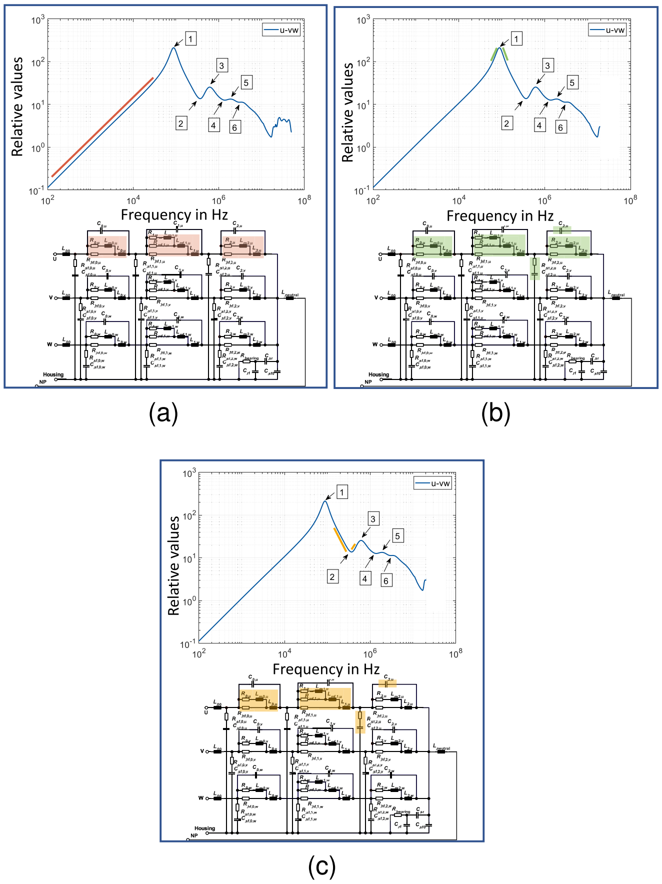

Fig. 5. Schematic explanation of the resonance behavior of the developed electrical circuit using the impedance amplitude spectrum. (a) Before the first resonance point. (b) Around the first resonance point. (c) Around the second resonance point.

is located between branch 2 and branch 0. In the following, phase U is used to explain the method of the proposed grey box model.

In branch 2 of phase U, the inductive and capacitive elements are drawn in different colors. The inductive part is modeled using an "RL"-ladder network to describe the frequency-dependent skin effect. This modeling approach is reported in many research studies concerning the high-frequency modeling of electrical machines. The capacitive part is further split into two parts, one for the winding-to-housing parasitic capacity and the other for the winding-to-winding parasitic capacity. In addition, an electrical resistor is added to model the insulation resistance between the winding and machine housing. The same explanation holds for the electrical circuit structure of branches 0 and 1.

B. Co-Relation Between the Impedance Spectra and the Equivalent Electrical Circuit

At low frequencies, all capacitances of a phase can be neglected due to their relatively high impedance amplitudes. Therefore, at low frequencies, all three branches of a phase can be approximated as a pure "RL"-ladder network. In this case, the resulting impedance increases with the frequency up until the first resonant point, as shown in Fig. 5(a).

With the increasing frequency, the capacitors in branch 2 start to compensate for the inductive part, which ultimately leads to the first resonant point. Further increase of the frequency leads to the reduction of the resulting impedance amplitude, as shown in Fig. 5(b). With higher frequency, the impedance of the inductive parts in branches 0 and 1 increases and starts to compensate for the capacitive part in branch 2. As a result, the second resonant point occurs and the impedance amplitude increases beyond it, as shown in Fig. 5(c). The occurrence of the remaining resonant points can be explained similarly. Namely, the capacitive part in branch 1 compensates for the inductive part in branch 1 and leads to resonant point 3, after which the amplitude decreases again. Similarly, the resonant points 4–6 can be interpreted.

Please note, unlike branches 0 and 2, the inductive part in branch 1 has three "RL" layers with the goal of modeling the frequency-dependent inductance and resistance in the medium frequency range more accurately.

TABLE II
MEANING OF THE SYMBOLS IN THE MODEL

Symbol	Meaning of the symbols
u,v,w	three phases
m	main or rather low-frequency
mf	middle-frequency
hf	high-frequency
0,1,2	branch 0, branch 1, branch 2
s	stator
r	rotor
f	frame or housing

C. Parameters of the Equivalent Electrical Circuit

The parameters $L_{,00}$ and $L_{,\text{neutral}}$ represent the inductances of the external supply lines that connect the PMSM under test during the impedance measurement. Additionally, the impedance between the stator winding and housing is represented for each branch by the parameters $R_{,\text{sf},i,j}$ and $C_{,\text{sf},i,j}$ ($i = 0, 1,$ and 2 and $j = u, v,$ and w). The value $C_{,\text{rf}}$ represents the capacitance between the housing and the rotor of the PMSM. The bearing resistance is represented by the symbol $R_{,\text{bearing}}$. The parameter $C_{,\text{sr}}$ represents the capacitance between the stator winding and the rotor surface. An overview of symbols is provided in Table II.

The grey box model illustrated in Fig. 4 contains 76 parameters in total that are to be fit. The similarities between the stator phases at high frequencies must be reflected in the parameters of the branches 0 and 1. In addition, the differences between the stator phases at low frequencies must be considered in the parametrization of components in branch 2. Therefore, branch 2 parameters must have a relatively large ratio between different phases. On the contrary, the parameters of branches 0 and 1 must have a relatively small ratio between different phases. Therefore, a grey box model with such relationships between the parameters as proposed is physically plausible and it promotes the capability of the model to be transferred to other applications as well.

D. Grey Box Model Improvement Using Mutual Inductances

In this article, we propose the utilization of the mutual inductances between the stator phases to further improve the accuracy of the grey box model. The proposed equivalent electrical circuit is provided in Fig. 6. The rationale for

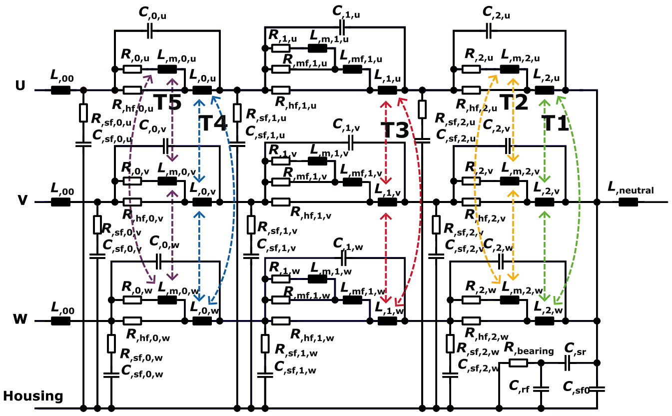

Fig. 6. Grey box model with mutual inductance between the phases. T1–T5 are five mutual inductances, symbolized with dashed lines in different colors.

TABLE III
COMPARISON OF MODELS WITH DIFFERENT NUMBER OF MUTUAL INDUCTANCES REGARDING THE AVERAGED RELATIVE DEVIATIONS Δ_{avg}

Topology	Amount of transformers				
	0	2	3	4	5
u-np	2.48 %	2.15 %	2.38 %	1.44 %	2.14 %
v-np	4.81 %	3.99 %	4.34 %	2.85 %	4.13 %
w-np	2.22 %	1.89 %	1.73 %	1.29 %	1.99 %
u-vw	4.62 %	4.38 %	3.92 %	1.14 %	3.85 %
v-wu	3.67 %	2.28 %	2.23 %	5.38 %	1.96 %
w-uv	3.72 %	5.61 %	5.46 %	2.59 %	4.48 %
u-gnd	1.23 %	1.24 %	1.26 %	1.61 %	1.68 %
v-gnd	2.00 %	1.73 %	1.72 %	1.57 %	2.01 %
w-gnd	1.73 %	1.95 %	1.90 %	1.46 %	1.87 %
u-v	2.31 %	2.95 %	2.67 %	1.15 %	2.73 %
v-w	1.61 %	4.15 %	4.22 %	2.63 %	3.40 %
w-u	6.65 %	6.43 %	5.72 %	1.78 %	5.27 %
uvw-gnd	4.31 %	3.41 %	3.23 %	1.71 %	3.49 %
$\overline{\Delta}_{avg}$	3.18 %	3.24 %	3.14 %	2.05 %	3.00 %

the mutual inductive coupling between phases of the stator winding is provided in the following.

The phases of a three-phase stator winding are spatially displaced by 120 electrical degrees. Therefore, there is an inductive coupling between the phases that should be considered. In this article, the included mutual inductances are symbolized by T1–T5 in different colors. The mutual inductance and the series-connected resistor form a ladder network similar to the well-known RL-ladder network. The frequency-dependent behavior of the mutual inductance is achieved by employing the resistor-mutual-inductance ladder network. Depending on the level of the model complexity, the number of considered mutual inductances can be varied. It is noteworthy to mention that each mutual inductance introduces three additional parameters, as three inductive coupling coefficients are required to represent a three-phase mutual inductor. For example, coupling coefficients $k_{uv,1}$, $k_{vw,1}$, and $k_{uw,1}$ are introduced to calculate the mutual inductance T1 between the phases in branch 2, as given in the following equations:

$$M_{uv,1} = k_{uv,1} \cdot \sqrt{L_{2,u} \cdot L_{2,v}} \tag{1}$$

$$M_{vw,1} = k_{vw,1} \cdot \sqrt{L_{2,v} \cdot L_{2,w}} \tag{2}$$

$$M_{uw,1} = k_{uw,1} \cdot \sqrt{L_{2,w} \cdot L_{2,u}}. \tag{3}$$

The differential evolution algorithm in [27] is utilized to fit the model parameters of the equivalent electrical circuit. The difference between the modeled and measured impedance spectra is considered with a cost function.

IV. Validation of Model in Frequency Domain

The validation of the proposed high-frequency models is first conducted for the PMSM placed on an isolated test bench and without considering the rotor position. Thereafter, the PMSM is placed on the grounded test bench and the validation of the impedance modeling is carried out while considering the rotor position.

A. PMSM on an Isolated Test Bench and With an Arbitrary Rotor Position

For high-frequency modeling validation of the PMSM in the frequency domain, the modeled impedance spectra are compared to the measured impedance spectra for different terminal configuration topologies, including phase–housing, phase–neutral point, phase–phase, and phase-to-phases. Indexes are introduced to calculate the deviation of the modeled impedance spectra relative to the measured impedance spectra, as defined in the following equations:

$$\Delta(f_i) = \left| \frac{\log(|Z_{\text{model}}(f_i)|) - \log(|Z_{\text{meas}}(f_i)|)}{\log(|Z_{\text{meas}}(f_i)|)} \right| \tag{4}$$

$$\Delta_{\text{sum}} = \sum_{i=1}^{n} \Delta(f_i) \tag{5}$$

$$\Delta_{\text{avg}} = \frac{\Delta_{\text{sum}}}{n}. \tag{6}$$

The parameter Δ_{avg}, as defined in (6), represents the average deviation in the modeled impedance spectrum from the measured impedance spectrum over the frequency range. It is calculated for different topologies, as introduced in Table I. In the formula for the parameter Δ_{avg}, the parameter n denotes the number of frequency values at which the impedance is measured.

The parameter $\overline{\Delta}_{avg}$, as defined in (7), represents the mean value of Δ_{avg} over different measurement topologies, whereby parameter N represents the total number of impedance measurement topologies. In Table III and Fig. 7, the mean deviations between the modeled and measured impedance spectra are given for the frequency range from 100 Hz to 5 MHz. As a result, the average deviation between the modeled and measured impedance spectra for all terminal configuration topologies is calculated to less than 4%

$$\overline{\Delta}_{\text{avg}} = \frac{\sum_{i=1}^{N} \Delta_{\text{avg}}(i\text{-th topology})}{N}. \tag{7}$$

The comparison of the grey box model with and without mutual inductance elements shows that the impedance modeling in the middle–high-frequency range improves with an increasing number of the mutual inductance elements although the mean errors between the grey box model with and without mutual inductance elements are similar.

The modeled impedance spectra using the grey box model without mutual inductance elements are compared to the measured impedance spectra, as illustrated in Fig. 8. The impedance fitting performance in phase-to-housing [Fig. 8(b)]

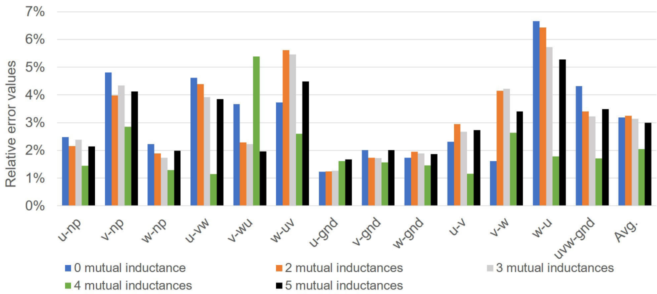

Fig. 7. Diagrammatic comparison of models with different number of mutual inductances regarding the relative deviations Δ_{avg}.

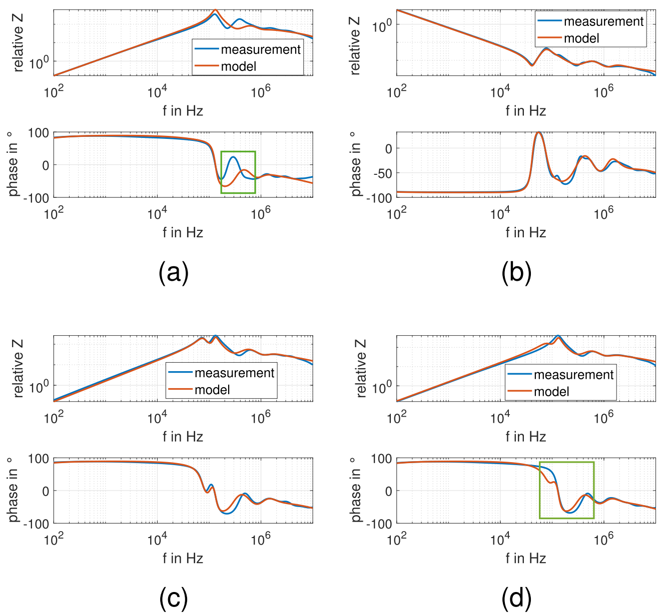

Fig. 8. Validation of impedance modeling without mutual inductances among phases in frequency domain with comparison to measured values: (a) V-NP; (b) U-housing; (c) U-V; and (d) V-WU.

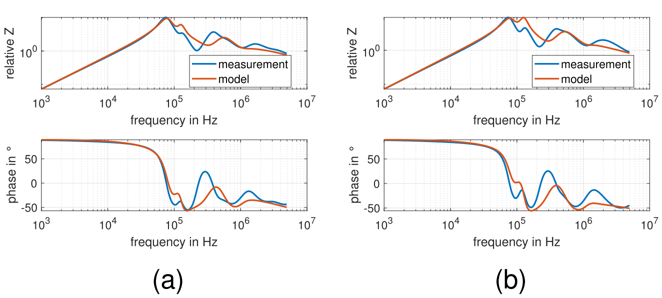

Fig. 9. Validation of phase–NP impedance modeling with four mutual inductances in frequency domain with comparison to measured values: (a) phase U to NP and (b) phase W to NP.

and phase-to-phase [Fig. 8(c)] indicates a higher degree of accuracy compared to the fitting results for phase-to-neutral point [Fig. 8(a)] and phase-to-phases [Fig. 8(d)]. In particular, relatively large phase deviations are observed in the frequency range from 50 to 500 kHz in the case of V-NP and V-WU modeled and measured impedance spectra.

As illustrated in Fig. 7, the impedance modeling results using the grey box model provide the least relative error for utilizing four mutual inductance elements. The corresponding results of modeling are shown in Figs. 9–11. The results presented in Fig. 9 refer to phase–NP impedance spectrum.

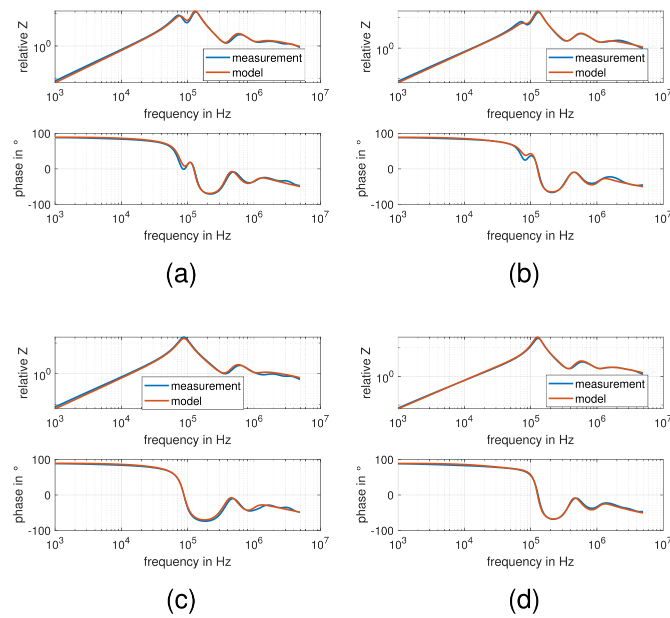

Fig. 10. Validation of phase–phase impedance modeling with four mutual inductances in frequency domain with comparison to measured values: (a) phase U-V; (b) phase V-W; (c) phase U-VW; and (d) phase V-WU.

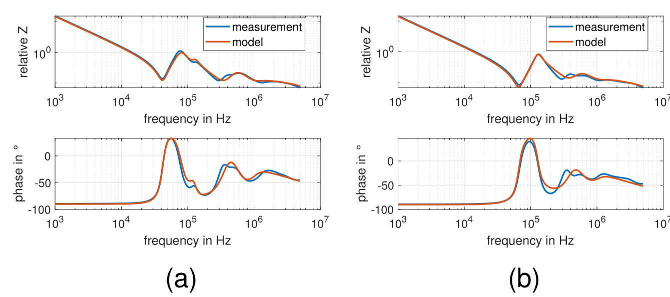

Fig. 11. Validation of phase–housing impedance modeling with four mutual inductances in frequency domain with comparison to measured values. (a) Phase U to housing. (b) Phase V to housing.

Fig. 10 illustrates the differential-mode impedance fitting results, while Fig. 11 shows the fitting results for phase-housing impedance.

Compared to Fig. 8(a), the level of accuracy regarding the phase–angle spectrum in the case of phase–NP topology is improved with utilizing four mutual inductance elements, as shown in Fig. 9. Furthermore, the differential-mode impedance spectra, as depicted in Fig. 10, match the measured spectra over a broad frequency range to a high degree of accuracy. As a result, the estimation of the differential-mode voltage at the machine terminals in inverter-fed operation can be achieved with accuracy. Moreover, the modeled phase–housing impedance spectra, as shown in Fig. 11, match the measured spectra to a large degree. Therefore, even the common-mode voltage and bearing currents are modeled with a high fidelity.

B. PMSM on a Grounded Test Bench With the Deterministic Rotor Position

In the following, the high-frequency modeling of the PMSM is conducted for different rotor positions, which are varied using a stepper motor, as illustrated in Fig. 2. First, the inductance of each phase is measured at 100 Hz and with

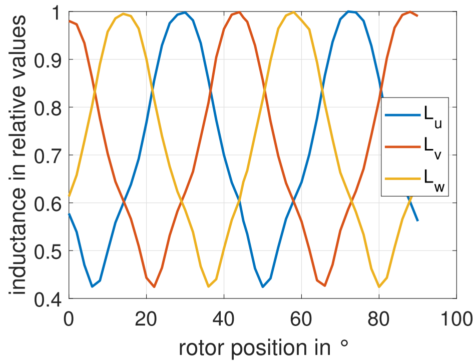

Fig. 12. Measured phase inductance dependent on rotor position.

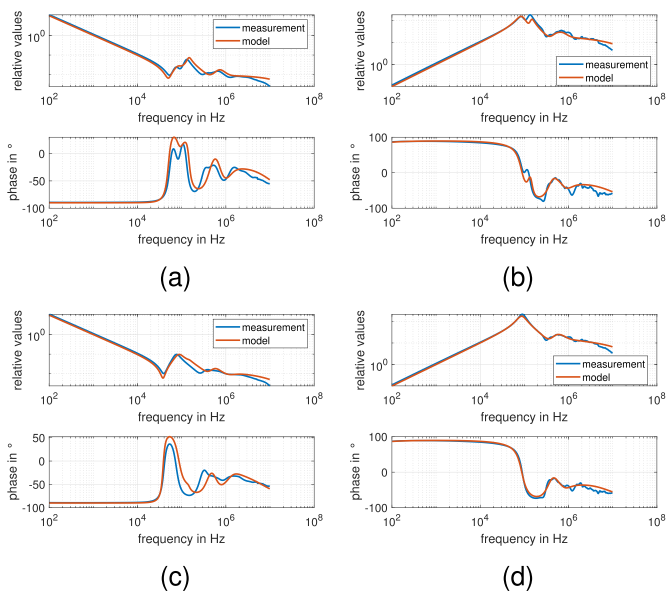

Fig. 13. Validation of impedance modeling in frequency domain with comparison to measured values at rotor position of 0°: (a) phase U–housing; (b) U-V; (c) phase V–housing; and (d) V-WU.

rotor position varying from 0° to 45° with an incremental step of 2°, as shown in Fig. 12. Since the PMSM has eight poles, the phase inductance has a magnetic periodicity of 45° mechanically. Furthermore, at the rotor position of 0°, the d-axis of the rotor is aligned with the magnetization axis of the V-phase winding, so that phase V inductance exhibits the maximum value.

Next, the impedance modeling is carried out for each rotor position using the corresponding impedance spectra. In the following, the impedance modeling results correspond to rotor positions of 0°, 22°, and 45° are presented. A comparison between modeled and measured impedance spectra for various rotor positions is provided in Figs. 13–15. Fig. 13 illustrates the modeling results for the rotor position of 0°, while Figs. 14 and 15 provide the modeling results for rotor positions of 22° and 45°, respectively. The accuracy of the proposed model with regard to common and differential modes is analyzed for four topologies, including U-housing, V-housing, U-V, and V-WU. After comparisons, it is evident that the modeled and measured impedance spectra match each other to a large degree in all rotor positions. This clearly shows the capability of the developed grey box method to be applied to other applications.

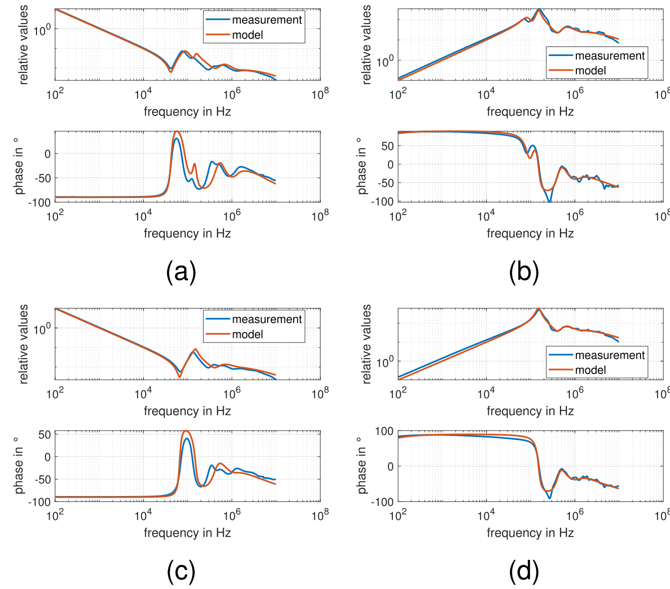

Fig. 14. Validation of impedance modeling in frequency domain with comparison to measured values at rotor position of 22°: (a) phase U–housing; (b) U-V; (c) phase V–housing; and (d) V-WU.

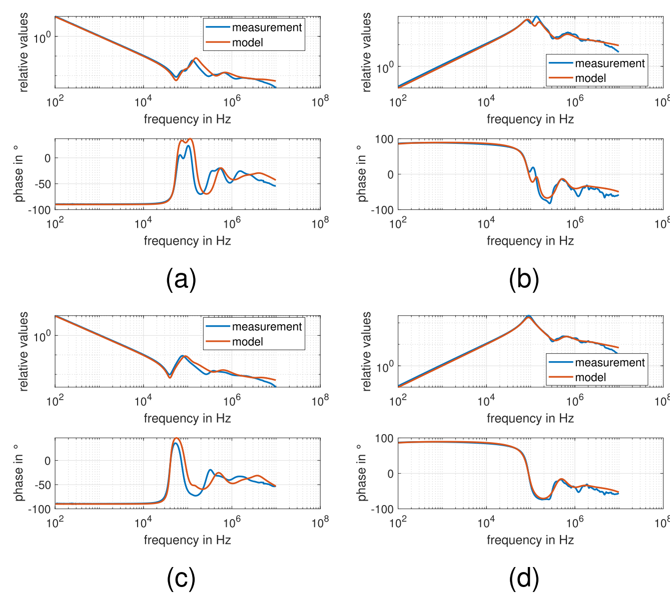

Fig. 15. Validation of impedance modeling in frequency domain with comparison to measured values at rotor position of 45°: (a) phase U–housing; (b) U-V; (c) phase V–housing; and (d) V-WU.

As evident from Figs. 13–15 compared to Figs. 10 and 11, the deviation between the modeled and measured impedances is larger in the case the rotor position is considered. However, the cause for the larger deviation is not the model itself. Rather, the test bench used for the case the rotor position is considered is grounded, as illustrated in Fig. 2. For this reason, the large metal surface of the test bench affects the equivalent impedance of the PMSM and distorts the impedance measurement accuracy because the metal surface behaves like an antenna. This is especially evident for impedance measurement above a few hundred kilohertz. This issue was addressed by inserting an insulating layer between the PMSM and the test bench. However, this deteriorating effect of the grounded test

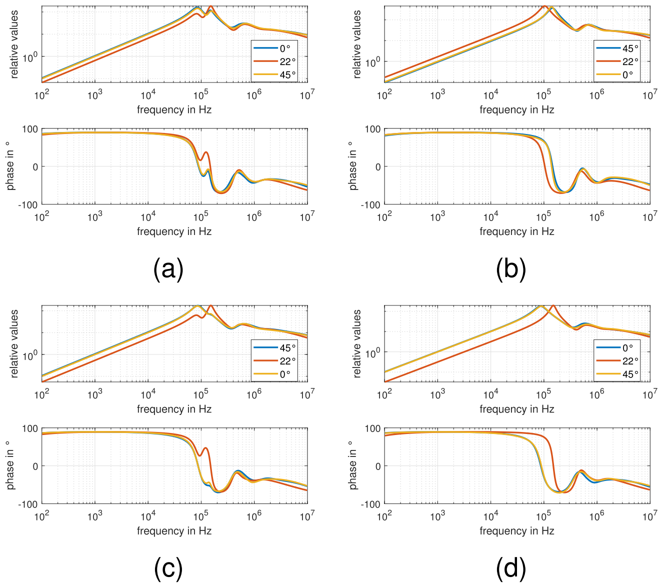

Fig. 16. Comparison of modeled impedance spectra among rotor position of 0°, 22°, and 45°: (a) U-V; (b) U-VW; (c) V-W; and (d) V-WU.

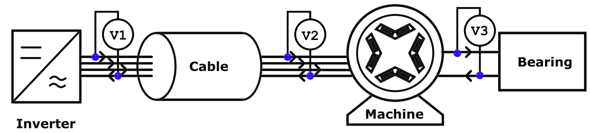

Fig. 17. Schematic presentation of the test bench with voltage measurement devices.

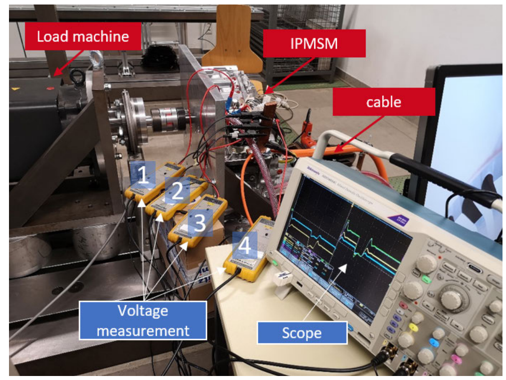

Fig. 18. Test bench and measurement configuration.

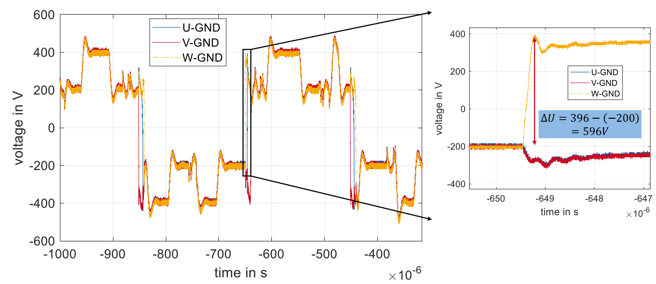

Fig. 19. Measured phase-to-housing voltage signals at the inverter output.

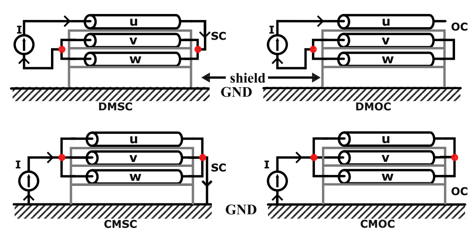

Fig. 20. Measurement setups for characterizing three-phase power cables with an outer shield.

bench could not be fully eliminated. The distorting effect of the test bench can be identified by observing Fig. 14(b), where the measured phase–angle reaches approximately −100° at a frequency of about 200 kHz, which is physically not possible for an electromagnetically passive system. In addition, the impedance spectrum measured on the grounded test bench exhibits higher fluctuations above 1 MHz compared to the impedance spectra measured on the insulated test bench. To conclude, to reduce the electromagnetic interference on the impedance measurement, the electrical machine should be isolated from the environment, i.e., test bench.

To emphasize the physical feasibility of the derived model that considers the rotor position, the modeled impedance spectra for rotor positions of 0°, 22°, and 45° are displayed in one figure, as shown in Fig. 16. It can be seen that the modeled impedance spectra for rotor angles of 0° and 22° exhibit the highest difference, while the impedance spectra for 0° and 45° are almost identical, as expected, as the PMSM has eight poles.

V. Validation of Model in Time Domain

In this section, validation of the proposed grey box model is conducted in time domain. First, the test bench for measuring characteristic voltages is introduced. To carry out the validation, a high-frequency model of the power cables is required. The modeling results of the cables are introduced. Finally, the validation in time domain is discussed.

A. Test Bench for Time-Domain Validation

The schematic configuration of the test bench for validating the grey box model of the PMSM in the time domain is shown in Fig. 17. The voltage signals at the inverter output and the PMSM terminals, such as the phase-to-phase voltage, the phase–housing voltage, and the neutral point–housing voltage, are measured. The actual configuration of the test bench is illustrated in Fig. 18, with four differential voltage probes and an oscilloscope. The phase-to-housing voltage signals at the output of the inverter are displayed in Fig. 19, and the voltage slew rate is approximately 3.3 kV/μs, which is the state-of-the-art value for an insulated-gate bipolar transistor (IGBT)-based power electronics inverter.

B. High-Frequency Modeling of Power Cables

A high-frequency model of power cables connecting the inverter and the motor is introduced to support the validation of the high-frequency modeling of the PMSM. Before modeling the cables, impedance measurements are carried out for different configuration setups, including differential-mode-short-circuit (DMSC), differential-mode-open-circuit (DMOC), common-mode-short-circuit (CMSC), and common-mode-open-circuit (CMOC), as shown in Fig. 20. The grey box model of the cables is illustrated in Fig. 21. The model contains 56 parameters in total.

The parametrization of the cable model is conducted using the same differential evolution algorithm as for the

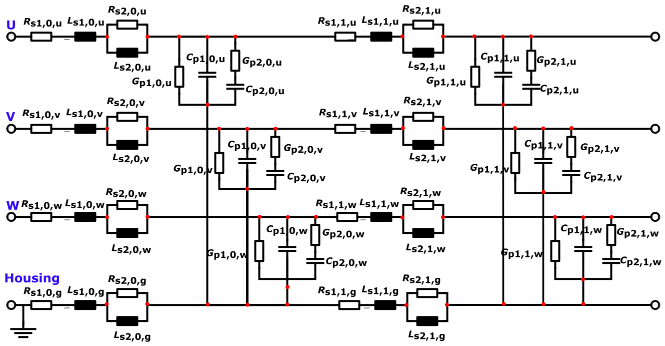

Fig. 21. Equivalent electrical circuit of the high-frequency cable model.

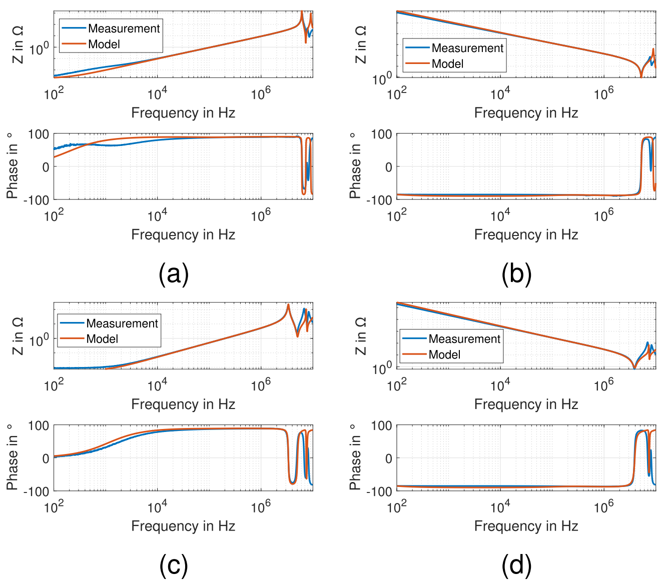

Fig. 22. Validation of the high-frequency model of power cables in frequency domain for configuration: (a) CMSC; (b) CMOC; (c) DMSC; and (d) DMOC.

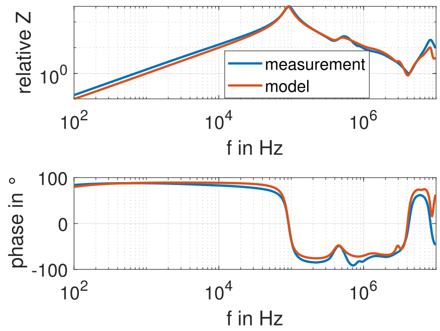

Fig. 23. Validation of the high-frequency modeling for the "U-VW" topology of the entire electrical drive consisting of the power cables and the PMSM.

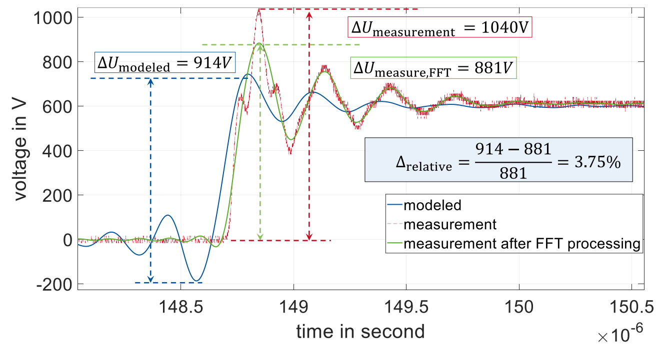

Fig. 24. Comparison between modeled and measured phase-to-phase voltages.

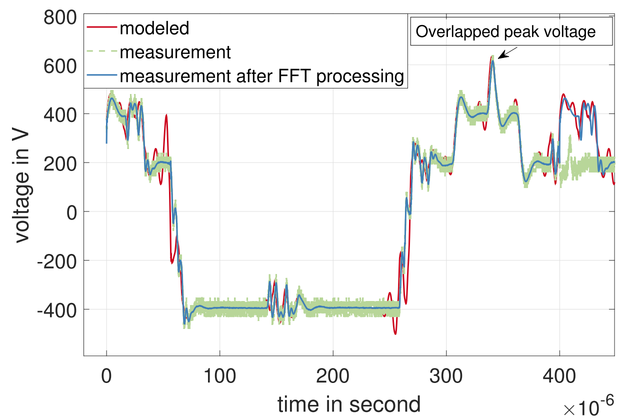

Fig. 25. Comparison between modeled and measured common-mode voltage between the neutral point and housing.

PMSM model. The particularities regarding the cable model structure and accompanying explanations will be presented in another work of the authors. Here, a comparison between the modeled and measured impedance spectra is provided in Fig. 22. As evident from Fig. 22, a high degree of accuracy for the cable model is achieved.

The next step is to validate the impedance of the electrical drive consisting of the power cables and the PMSM in the frequency domain. In Fig. 23, the modeled impedance spectrum of the entire system matches the measured spectrum to a large degree, which means that both high-frequency models of the power cables and PMSM are correct over a wide frequency range.

C. Time-Domain Validation of the Grey Box Model of PMSM

Validation of the high-frequency model regarding differential-mode voltage in time domain is illustrated in Fig. 24. The measurement on the test bench is performed for the following operating point: the dc-link voltage is 600 V and the PMSM rotational speed is 500 min^{-1}.

The modeled phase–phase voltages are compared to the measured voltage profiles. The comparison is conducted based on both: the raw signal data recorded in time domain with a high sampling rate and postprocessed voltage signal after applying the Fourier transformation. The order number of the Fourier series is set to be 1000 times higher than the switching frequency, which is 3 kHz, to keep the computational burden affordable. As a result, the measured voltage signal after applying the Fourier transformation has a lower peak value than the original measured value at some time points.

The comparison indicates that the modeled phase-to-phase voltage peak ΔU is 914 V, which is about 3.75% higher compared to the measured voltage peak of 881 V. Regarding the oscillation frequency following the switching transient, the modeled voltage oscillation frequency is 3.6 MHz, which is close to the frequency of the measured voltage signal of 3.4 MHz. It can be concluded that the high-frequency model of the PMSM has a high degree of fidelity for the

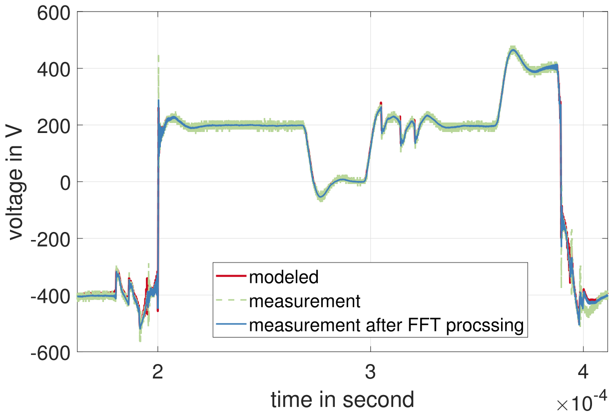

Fig. 26. Comparison between modeled and measured phase–housing voltage on the motor side.

differential-mode voltage. Therefore, the grey box model can be used to estimate the differential-mode voltages in inverter-fed electrical machines.

Validation of the grey box model regarding the common-mode voltage is illustrated in Figs. 25 and 26. The modeled and measured voltage signals between the neutral point and housing are compared in Fig. 25. The modeled and measured voltage signals between the machine terminals and housing are illustrated in Fig. 26. Also, in the case for common-mode voltage, a high degree of fidelity is evident.

VI. Conclusion

A universal grey box model is developed for high-frequency modeling of PMSM with interior permanent magnets by considering the frequency-dependent mutual impedance between phases. The model parameters are fit considering the similarity between the phases in high-frequency range and their difference in low-frequency range. The high-frequency model of the PMSM is validated in the frequency domain with an averaged relative error of less than 4% for the frequency range from 100 Hz to 5 MHz. Additionally, the model is also validated in the time domain based on the test bench measurements, and a relative error of 3.75% is observed in the phase-to-phase voltage. For the common-mode voltage, the measured and modeled voltage signals match each other in peak values and oscillation frequencies during switching transients of semiconductor elements. Therefore, this model can be used with a high degree fidelity to estimate the maximum voltage stress in the insulation system of a PMSM. Moreover, the proposed grey box model can be utilized to improve the insulation system design in the next generation of the analyzed PMSM. In the future, the model will also be applied to model electrical machines without an accessible neutral point.

Acknowledgment

The authors express the memory and gratitude to Isabel Mainz.

References

[1] O. J. Tola, J. G. Ambafi, E. A. Umoh, and O. E. Osinowo, "Performance analysis of a PMSM for traction applications in electric vehicles with hairpin winding technology," in *Proc. IEEE Nigeria 4th Int. Conf. Disruptive Technol. Sustain. Develop. (NIGERCON)*, Apr. 2022, pp. 1–5.

[2] G. Venturini, M. Carbonieri, L. Di Leonardo, and M. Popescu, "Hairpin windings for traction machines: Analysis and comparison," in *Proc. Int. Conf. Electr. Mach. (ICEM)*, Sep. 2022, pp. 1655–1661.

[3] A. Torrisi and D. Brunelli, "High dv/dt pulse generator based on series-connetion SiC MOSFETs," in *Proc. Int. Symp. Power Electron., Electr. Drives, Autom. Motion (SPEEDAM)*, Jun. 2022, pp. 528–533.

[4] Y. Xie, J. Zhang, F. Leonardi, A. R. Munoz, M. W. Degner, and F. Liang, "Modeling and verification of electrical stress in inverter-driven electric machine windings," *IEEE Trans. Ind. Appl.*, vol. 55, no. 6, pp. 5818–5829, 2019.

[5] A. H. Bonnett, "Analysis of the impact of pulse-width modulated inverter voltage waveforms on AC induction motors," *IEEE Trans. Ind. Appl.*, vol. 32, no. 2, pp. 386–392, Apr. 1996.

[6] D. Han, S. Li, Y. Wu, W. Choi, and B. Sarlioglu, "Comparative analysis on conducted CM EMI emission of motor drives: WBG versus Si devices," *IEEE Trans. Ind. Electron.*, vol. 64, no. 10, pp. 8353–8363, Oct. 2017.

[7] G. Almandoz, S. Zarate, A. Egea, Y. Moreno, A. Urdangarin, and R. Moreno, "High frequency modeling of electric drives for electromagnetic compatibility analysis," in *Proc. Int. Conf. Electr. Mach. (ICEM)*, vol. 1, Aug. 2020, pp. 1129–1135.

[8] H. Zeng, J. Swanke, T. M. Jahns, and B. Sarlioglu, "High-frequency modeling and inter-turn voltage distribution analysis of a modular electric machine for electric aircraft propulsion," in *Proc. IEEE Transp. Electrific. Conf. Expo (ITEC)*, Jun. 2022, pp. 1097–1104.

[9] Y. Xu et al., "Impact of high switching speed and high switching frequency of wide-bandgap motor drives on electric machines," *IEEE Access*, vol. 9, pp. 82866–82880, 2021.

[10] R. Kerkman, D. Leggate, and G. Skibinski, "Interaction of drive modulation and cable parameters on ac motor transients," in *Proc. IEEE Ind. Appl. Conf. 31st IAS Annu. Meeting (IAS)*, vol. 1, Oct. 1996, pp. 143–152.

[11] M. Ghassemi, "Accelerated insulation aging due to fast, repetitive voltages: A review identifying challenges and future research needs," *IEEE Trans. Dielectr. Electr. Insul.*, vol. 26, no. 5, pp. 1558–1568, Oct. 2019.

[12] J. Dittmann, C.-N. Behrendt, and B. Ponick, "Prediction of the voltage distribution in a inverter-fed hairpin stator winding," in *Proc. 25th Int. Conf. Electr. Mach. Syst. (ICEMS)*, Nov. 2022, pp. 1–6.

[13] J. Dittmann, M. England, and B. Ponick, "Design of hairpin windings considering the transient potential distribution," *E&I Elektrotechnik Informationstechnik*, vol. 140, no. 2, pp. 271–280, 2023.

[14] N. Driendl, F. Pauli, and K. Hameyer, "Characterization of insulation material parameters in low-voltage electrical machines," in *Proc. Int. Conf. Electr. Mach. (ICEM)*, Sep. 2022, pp. 1314–1320.

[15] O. Magdun, S. Blatt, and A. Binder, "Calculation of stator winding parameters to predict the voltage distributions in inverter fed AC machines," in *Proc. 9th IEEE Int. Symp. Diag. Electric Mach., Power Electron. Drives (SDEMPED)*, Aug. 2013, pp. 447–453.

[16] X. Ju et al., "Voltage stress calculation and measurement for hairpin winding of EV traction machines driven by SiC MOSFET," *IEEE Trans. Ind. Electron.*, vol. 69, no. 9, pp. 8803–8814, Sep. 2022.

[17] S. Sundeep, J. Wang, and A. Griffo, "Holistic modeling of high-frequency behavior of inverter-fed machine winding, considering mutual couplings in time domain," *IEEE Trans. Ind. Appl.*, vol. 57, no. 6, pp. 6044–6057, Nov. 2021.

[18] R. L. Stoll, *The Analysis of Eddy Currents*. Oxford, U.K.: Clarendoon Press, 1974, pp. 4–6.

[19] M. S. Toulabi, L. Wang, L. Bieber, S. Filizadeh, and J. Jatskevich, "A universal high-frequency induction machine model and characterization method for arbitrary stator winding connections," *IEEE Trans. Energy Convers.*, vol. 34, no. 3, pp. 1164–1177, Sep. 2019.

[20] A. Hoffmann and B. Ponick, "Statistical deviation of high-frequency lumped model parameters for stator windings in three-phase electrical machines," in *Proc. Int. Symp. Power Electron., Electr. Drives, Autom. Motion (SPEEDAM)*, Jun. 2020, pp. 85–90.

[21] V. Karakasli, F. Gross, T. Braun, H. De Gersem, and G. Griepentrog, "High-frequency modeling of delta- and star-connected induction motors," *IEEE Trans. Electromagn. Compat.*, vol. 64, no. 5, pp. 1533–1544, Oct. 2022.

[22] Y. Wu, H. Li, W. Ma, M. Dong, and Q. Zhong, "High-frequency model of permanent magnet synchronous motor for EMI prediction in adjustable speed drive system," in *Proc. IEEE Int. Power Electron. Appl. Conf. Expo. (PEAC)*, Nov. 2018, pp. 1–6.

[23] Y. Wu et al., "High-frequency modelling of permanent magnet synchronous motor with star connection," *IET Electr. Power Appl.*, vol. 12, no. 4, pp. 539–546, Apr. 2018.
[24] B. Heidler, K. Brune, and M. Doppelbauer, "High-frequency model and parameter identification of electrical machines using numerical simulations," in *Proc. IEEE Int. Electric Mach. Drives Conf. (IEMDC)*, May 2015, pp. 1221–1227.
[25] A. Hoffmann and B. Ponick, "Method to predict the non-uniform potential distribution in random electrical machine windings under pulse voltage stress," *Energies*, vol. 15, no. 1, p. 358, Jan. 2022.
[26] Y. Xie, J. Zhang, F. Leonardi, A. R. Munoz, and M. W. Degner, "Investigation of surge voltage propagation in inverter-driven electric machine windings," *IEEE Trans. Ind. Electron.*, vol. 70, no. 10, pp. 9811–9822, Oct. 2023.
[27] Y. Zhang, H. Peng, and W. Hofmann, "Transient skin effect in highly dynamic induction motor drives: Energy-optimized design," *Electr. Eng.*, vol. 105, no. 2, pp. 1015–1024, Apr. 2023.

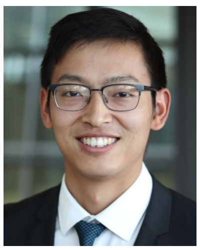

Hujun Peng received the bachelor's degree in electrical engineering from Zhejiang University, Hangzhou, China, in 2013, the master's degree in electrical engineering from the Dresden University of Technology, Dresden, Germany, in 2017, and the Ph.D. degree, from RWTH Aachen University, Aachen, Germany, in 2023.

Since April 2018, he has been working as a Research Assistant with the Institute of Electrical Machines, RWTH Aachen University, Aachen, Germany, where he has been working as a Post-Doctoral Researcher, since 2023. His research interests include the high-frequency modeling of electrical machines, energy management of fuel cell hybrid vehicles characterization of insulation systems in electric machines, and the analysis of parasitic effects in electric drives.

Niklas Driendl received the M.Sc. degree in electrical engineering from RWTH Aachen University, Aachen, Germany, in 2018.

He joined the Institute of Electrical Machines, RWTH Aachen University, as a Research Associate, in January 2019. His research interests include the characterization of insulation systems of electrical machines, the modeling of partial discharge processes, and the analysis of aging processes.

Svetomir Stevic (Graduate Student Member, IEEE) received the Diploma degree from the School of Electrical Engineering, University of Belgrade, Belgrade, Serbia, in 2011, and the M.Sc. degree in electrical engineering from RWTH Aachen University, Aachen, Germany, in 2016.

From 2016 to 2018, he worked with the Idaho National Laboratory, Idaho Falls, ID, USA, on topics including the design, modeling, and simulation of power converters, energy devices and power grids, as well as controller- and power-hardware-in-the-loop tests for intelligent power grids. Since August 2018, he has been working with the Institute of Electrical Machines, RWTH Aachen University, on topics including co-design, prototyping, and control of power electronics and electrical machines, as well as the analysis of interaction mechanisms in electrical drives.

Daniel Butterweck received the M.Sc. degree in electrical engineering from RWTH Aachen University, Aachen, Germany, in 2013.

Since January 2014, he has been working as a Research Associate with the Institute of Electrical Machines (IEM), RWTH Aachen University, where he led the Automotive Research Group, from 2017 to 2018. Since March 2018, he has been working as a Chief Engineer with IEM. His research focuses on the design and simulation of electrical drivetrains and machines.

Yousef Firouz received the Ph.D. degree in engineering sciences from Vrije Universiteit Brussel, Brussels, Belgium, in 2019. His Ph.D. thesis entitled "Advanced System Identification and Modelling of Lithium-Ion Batteries in the Time and Frequency Domains."

He is currently a Research Engineer with Toyota Motor Europe, Zaventem, Belgium. His fields of expertise include characterization, electrothermal and electrochemical modeling of Li-ion batteries, high-frequency electric machine modeling, and power electronics.

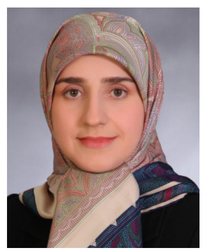

Leila Sharifian received the master's degree from the Sharif University of Technology, Tehran, Iran, in 2004, and the Ph.D. degree in mechanical and process engineering from the Swiss Federal Institute of Technology, Zürich, Switzerland, in 2011.

After that, she worked as a Post-Doctoral Researcher with the Swiss Federal Institute of Technology. Since 2012, she has been working with Toyota Motor Europe, Zaventem, Belgium, where she is currently a Technical Manager of powertrain digital, E-motor predevelopment, and battery electric vehicle (BEV) thermal management system improvement. Her research interests include electric motors, gasoline engines, battery and system thermal management, and diesel engines.

Kay Hameyer (Senior Member, IEEE) received the M.Sc. degree in electrical engineering from the University of Hannover, Hanover, Germany, in 1986, and the Ph.D. degree from the University of Technology Berlin, Berlin, Germany, in 1992, working on permanent magnet excited machines.

He worked as a Design Engineer of permanent magnet servo motors with Robert Bosch GmbH, Stuttgart, Germany. From 1988 to 1993, he was a Member of Staff with the University of Technology Berlin. From 1996 to 2004, he was a Full Professor of numerical field computations and electrical machines with Katholieke Universiteit Leuven (KU Leuven), Leuven, Belgium. Since 2004, he has been a Full Professor and the Director of the Institute of Electrical Machines (IEM), RWTH Aachen University, Aachen, Germany. The characterization and modeling of hard- and soft-magnetic materials are another focus of his work. He has authored or coauthored more than 350 journal publications, more than 700 international conference publications, and four books. His research interest focuses on all aspects of the design, control, and manufacturing of electrical machines and the associated numerical simulation. His research interests include numerical field computation and optimization, and the design and control of electrical machines, in particular, permanent magnet excited machines and induction machines.

Dr. Hameyer is a member of the German VDE and a fellow of the Institution of Engineering and Technology, U.K.